Beta-connectin studied by Small-Angle X-rays Scattering and Single Molecule Force Spectroscopy by AFM

β-connectin studies by small-angle x-ray scattering and single-molecule force spectroscopy by atomic force microscopy

S. Marchetti,[1] F. Sbrana,[2] A. Toscano,[3] E. Fratini,[4] M. Carlà,[1] M. Vassalli,[2] B. Tiribilli,[5] A. Pacini,[3] and C. M. C. Gambi[1]

[1]*Department of Physics, University of Florence and CNISM Via G. Sansone 1, IT-50019, Sesto Fiorentino (Florence), Italy*

[2]*Biophysics Institute of the National Research Council, Via De Marini 6, Genova, Italy*

[3]*Department of Anatomy, Histology, and Forensic Medicine, University of Florence, Florence, Italy*

[4]*Department of Chemistry and Consorzio Interuniversitario per lo Sviluppo dei Sistemi a Grande Interfase (CSGI), University of Florence, Via della Lastruccia 3, IT-50019, Sesto Fiorentino (Florence), Italy*

[5]*Complex System Institute of the National Research Council (ISC-CNR), Sesto Fiorentino (Florence), Italy*

(Received 27 July 2010; revised manuscript received 12 April 2011; published 24 May 2011)

The three-dimensional structure and the mechanical properties of a β-connectin fragment from human cardiac muscle, belonging to the *I* band, from I_{27} to I_{34}, were investigated by small-angle x-ray scattering (SAXS) and single-molecule force spectroscopy (SMFS). This molecule presents an entropic elasticity behavior, associated to globular domain unfolding, that has been widely studied in the last 10 years. In addition, atomic force microscopy based SMFS experiments suggest that this molecule has an additional elastic regime, for low forces, probably associated to tertiary structure remodeling. From a structural point of view, this behavior is a mark of the fact that the eight domains in the I_{27}-I_{34} fragment are not independent and they organize in solution, assuming a well-defined three-dimensional structure. This hypothesis has been confirmed by SAXS scattering, both on a diluted and a concentrated sample. Two different models were used to fit the SAXS curves: one assuming a globular shape and one corresponding to an elongated conformation, both coupled with a Coulomb repulsion potential to take into account the protein-protein interaction. Due to the predominance of the structure factor, the effective shape of the protein in solution could not be clearly disclosed. By performing SMFS by atomic force microscopy, mechanical unfolding properties were investigated. Typical sawtooth profiles were obtained and the rupture force of each unfolding domain was estimated. By fitting a wormlike chain model to each peak of the sawtooth profile, the entropic elasticity of octamer was described.

DOI: 10.1103/PhysRevE.83.051919 PACS number(s): 87.14.E−, 87.15.B−, 87.64.Bx, 87.64.Dz

I. INTRODUCTION

β-connectin, also called titin, is a large filamentous protein with molecular mass 3 MDa, length 900 nm, and diameter 40 Å [1,2], and is composed of elastic (*I* band) and inelastic (*A* band) parts. Despite its immense size, the secondary and tertiary structures of the molecule are relatively simple: more than 90% consists of immunoglobulinlike domains (Ig) and fibronectin-type-III-like domains (FnIII).

Both Ig and FnIII modules are mainly organized into β sheets folded to form a compact structure, stabilized by cooperative hydrogen bonds [3]. In particular, each Ig domain folds into a β sandwich, containing eight β sheets, and can be considered an ellipsoid (43 Å; 21 Å; 21 Å), as reported in the Protein Data Bank [4].

In vertebrate organisms, β-connectin has a crucial role in which it confers passive elasticity to muscles [5]. In other words, this protein is subject to external forces during muscle contraction and it behaves like an elastic spring, providing a resistance to the stress proportional to its intensity and rapidly recovering to the original state upon removal of the external stimulus. The structural basis of this behavior has been studied and it has been found that at least three regimes can be identified, depending on the external force. For very low forces, the tertiary structure of the protein is involved, leading to a straightening of the protein domains subject to the tension. After this phase, the unordered regions of the protein, mainly the so-called Pro-Glu-Val-Lys (PEVK) region, come into play by providing a full entropic elastic resistance. Finally, the Ig-like and FnIII-like domains start unfolding, absorbing the shock and avoiding the onset of molecular damages. Whereas the second and third regimes have been extensively characterized, the first one, associated to domain-domain interactions, has not yet been fully described. Only recently, the structure of an Ig-like hexamer obtained from β-connectin has been studied by small angle x-ray scattering (SAXS), showing a nonrandom three-dimensional organization of the domains [6] that has been successively associated to the low forces elasticity of the molecule by molecular dynamics simulations [7].

In this paper, the three-dimensional structure and elastic properties of octamer from β-connectin belonging to the *I* band, from I_{27} to I_{34}, are addressed. This molecule has been previously studied by means of single-molecule force spectroscopy (SMFS) experiments (see, e.g., [8,9]) and the same experimental approach was used here to have an insight into the elastic behavior of the protein. The presence of a mechanical response in the low forces regime is probably associated to a well-defined three-dimensional structure in solution. This hypothesis has been deeply investigated by means of SAXS technique, and the outcome of the experiments has been compared with assessed theoretical models.

In this paper, by investigating concentrated and dilute octamer solutions, we have found in the latter solution both aggregates and single octamers. In a previous paper [10], dynamic light scattering (DLS) and atomic force microscopy (AFM) imaging on octamer and tetramer fragments of β-connectin from human cardiac muscle were used to investigate the protein's folding-unfolding process. DLS provided

the protein's size as a function of temperature up to 86 °C. The results provide evidence that thermal denaturation was shown for octamer and tetramer fragments as a function of temperature increase, followed by aggregation. At low scattering angles in the thermal interval 20–40 °C, the aggregates are present in small amounts (about 9%), whereas, at higher temperatures (60–80 °C), they are present in greater amounts (7%–97%). Furthermore, aggregates were also detected by AFM techniques. DLS and SMFS by AFM results agreed in measuring the size of both single octamers and corresponding aggregates. In this paper, the I_{27}-I_{34} octamer's fragment of the elastic I band is investigated from both points of view of microstructure and force applied to a single biomolecule as a function of extension by SAXS and SMFS by AFM. Our results suggest in which way the Ig domains are assembled in a modular protein such as β-connectin and whether the consecutive Ig domains are free to move with respect to one another, leading to the reorganization of the shape and the structure of the whole protein.

II. MATERIALS AND SAMPLE PREPARATION

β-connectin fragments were prepared as detailed in Appendix A and stored at 4 °C. All measurements were performed at $T = 20$ °C. The reported preparation method assures that octamers in aqueous solution are the output of the affinity chromatography procedure. Two samples of octamer were measured by SAXS. One, named dilute, was obtained as reported in Appendix A. The other, named concentrated, was obtained from the dilute sample by a diafiltration process, using an Amicon ultrafiltration stirred cell [model 8003, Millipore Corporation Cat. No. 5125 mounting a membrane of regenerated cellulose, 10 kDa NmWL (Ultracell YM10)].

The octamer's final concentration was checked by absorbance measurements at 280 nm in 0.1-cm Hellma cells with a UV spectrophotometer (Perkin-Elmer Lambda 900), assuming a molar extinction coefficient of 60 880 M^{-1} cm^{-1} at this wavelength. This value was estimated by the method of Gill and von Hippel [11] from knowledge of protein amino acid composition by the Protein Calculator v3.3 [12].

The octamer charge is negative (see caption of Table I). The octamer's solution was filtered with a 0.22-μm filter before and after the concentration step. The final fragment concentrations of dilute and concentrated samples were 50 and 230 mg/ml, respectively. The samples are at the same pH value of 7.3, as reported in Appendix A.

The x-ray scattering length density of the octamer is $\rho_o = \frac{N_e N_A}{M_o v_o} r_e = 1.223 \times 10^{-5}$ Å^{-2}, where $N_e = 45\,290$ is the total number of electrons present in the octamer, N_A is the Avogadro number, $r_e = 2.82 \times 10^{-5}$ Å is the classical radius of electron, $M_o = 85$ kDa is the octamer molecular weight, and v_o is its partial specific volume. It is a common practice to assume that most of globular proteins have a similar partial specific volume. As suggested by Svergun and Mylonas [13], the effective value of $v_o = 0.7425$ cm^3 g^{-1} provides sufficiently good accuracy on average within 10% for most globular proteins. The x-ray scattering length density of solvent, i.e., water, is $\rho_s = \frac{N_e N_A}{M_s v_s} r_e = 9.38 \times 10^{-6}$ Å^{-2}. In this case, $N_e = 10$, $M_s = 18$ Da, and $v_s = 1$ cm^3 g^{-1}.

In the SMFS by AFM experiments, the octamers were kept in phosphate-buffered saline solution (PBS). The octamer concentration was 50 mg/ml.

III. METHODS

A. Small-angle x-ray scattering

SAXS measurements were carried out with a HECUS SWAX-camera (Kratky) equipped with a position-sensitive detector (OED 50M) containing 1024 channels of width 54 μm. Cu K-α radiation of wavelength λ = 1.542 Å was provided by a Seifert ID-3003 x-ray generator (sealed-tube type), operating at a maximum power of 2 kW. A 10-μm-thick nickel filter was used to remove the Cu K-β radiation. The sample-to-detector distance was 273 mm. The volume between the sample and the detector was kept under vacuum during the measurements to minimize scattering from the air. The Kratky camera was calibrated in the small-angle region using silver behenate having (001) interplanar long-period spacing $D = 58.38$ Å [14].

Scattering curves were obtained in the Q-range between 0.01 and 0.54 Å^{-1}, with Q being the scattering wave vector $Q = (4\pi/\lambda)\sin(\theta)$, and 2θ the scattering angle. Samples were filled into a 1-mm quartz capillary. All the SAXS measurements have been performed at $T = 20 \pm 0.1$ °C.

TABLE I. Fitting results according to a globular conformation interacting by a long-range repulsion potential. The negative sign of the octamer charge comes from the consideration that the pI of the octamer (5.8) is lower than the experimental pH = 7.3.

		Dilute	Concentrated
Charge	Z	−13.0	−13.0
Major semiaxis (Å)	a_p	33.0	33.6
Minor semiaxis (Å)	b_p	13.6	12.9
Axial ratio	$\nu = a_p/b_p$	2.4	2.6
Shell thickness (Å)	t	24.4	7.35
Ratio	$r = \rho_{sh}/\rho_s$	1.06	1.09
Effective hard sphere diameter (Å)	σ_H	49.1	48.8
Reduced screening parameter	$k = \kappa\sigma_H$	3.24	8.80
Debye length (Å)	l_D	15.2	5.5
Contact potential (k_BT)	γe^{-k}	1.74	0.63

All scattering curves were corrected for the solvent and cell contribution considering the relative transmission factors. SAXS curves were iteratively desmeared using the procedure reported by Lake [15]. Short time acquisitions on fresh samples were used in order to check that radiation damage was not induced by x-ray exposition.

B. Single-molecule force spectroscopy experiments

SMFS experiments were carried out using a PicoSPM AFM microscope (Agilent technologies, CA, USA). CSG01 rectangular contact cantilevers by NT-MDT (Moscow, Russia) were used. The spring constant of each probe was measured by using a thermal calibration procedure, and only the probes with a spring constant lower than 0.03 N/m were used. The octamers were allowed to adsorb onto a freshly evaporated gold surface by placing a drop of 20 μl of sample waiting for 10 min. The sample was gently rinsed with phosphate-buffered saline solution (PBS 1×) to remove any free octamer. Mechanical unfolding experiments were performed drawing up and moving the probe away from the substrate at a constant pulling speed of 800 nm/s in PBS at room temperature. Force-extension curves were recorded, observing the characteristic sawtooth pattern from which the force needed to unfold each domain was measured.

1. Single-molecule force spectroscopy data analysis

Force versus extension curves $F(d)$ were corrected for hysteresis and nonlinear effects (e.g., interference on the optical path) and thus converted into force versus distance curves $F(z)$ after determination of the contact point. The initial, noisy part of the curve, associated to aspecific adhesion of the protein with the substrate, was discarded. The resulting sawtooth pattern was analyzed using the wormlike chain (WLC) model of pure-entropic elasticity according to the following equation [16]:

$$F(z) = \frac{k_B T}{L_p}\left[\frac{1}{4\left(1-\frac{z}{L_c}\right)^2} - \frac{1}{4} + \frac{z}{L_c}\right], \qquad (1)$$

where F is the unfolding force, z is the end-to-end extension, T is the temperature, k_B is the Boltzmann constant, L_c is the polymer contour length, and L_p is its persistence length (a measure of the bending rigidity of the polymer chain, the shorter L_p, the weaker the chain). In order to stabilize the fitting procedure, the persistence length was fixed at a value of $L_p = 0.4$ nm [8] and the adjustable parameter L_c was estimated by fitting the WLC model to the rising edge of each peak in the force-extension profile. The contour length increment ΔL_c between two consecutive unfolding peaks was calculated and the last peak, associated to detachment of the protein from the tip, was not taken into account in the analysis.

IV. RESULTS

A. Single-molecule force spectroscopy

The mechanical unfolding properties of the octamer were investigated by AFM based single-molecule force spectroscopy. In a typical AFM pulling experiment, a single molecule, adsorbed onto the gold substrate, is picked up and stretched, recording the resulting force until it detaches from the probe tip. During the experiment, single Ig-like domains are subject to a rising force that lowers the energy barrier between the folded and the unfolded state of the domain, until it abruptly opens, giving rise to a characteristic jump in the curve (see Fig. 1). The sequential opening of all the domains results in a sawtoothlike pattern that is a clear sign that the pulled molecule is a single octamer [8].

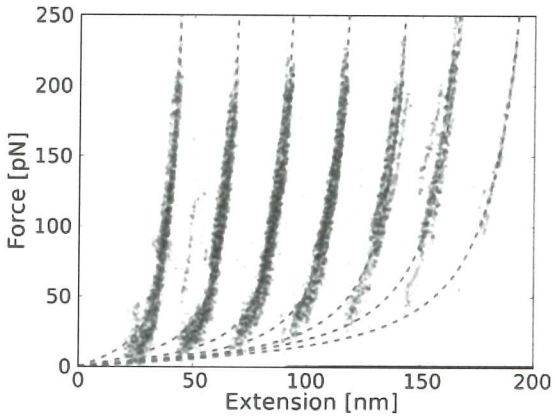

FIG. 1. (Color online) Sawtooth pattern. A set of 12 force-extension curves with more than 5 peaks are presented (dots). The dashed lines are WLC fits with L_p fixed at 0.4 nm and L_c set at the mean value between all curves.

The number of force peaks within each stretching experiment varied from two to eight peaks due to the random pickup of the tip in the fragment. In the data analysis, we considered only the curves showing at least five peaks. Multimolecule stretching and all other spurious events were rejected. In Fig. 1, a set of 12 stretching curves with more than 5 stretching events is shown. The characteristic sawtooth pattern shape with equally spaced peaks is stable and reproducible. The maximum rupture force of each peak and the mean increase in the contour length were estimated, obtaining $F_{peak} = 237 \pm 65$ pN and $\Delta L_c = 24.7 \pm 3.7$ nm. They are in good agreement with the lengths reported in the literature for domain unfolding events of I_{27}-I_{34} [8].

The unfolding of a protein domain is a strong event occurring in the stretching of the molecule and, from a physiological point of view, it confers to the molecule the ability to sustain high forces, elongating one or more domains and recovering its original state after removal of the external stress. But, as mentioned, Ig-like domains are claimed to provide also a second type of elasticity to the molecule, for lower forces regimes, associated to the interaction between modules. The sensitivity of AFM based single-molecule force spectroscopy could be enough to observe such a phenomenon, but it lies in a region of the force curve that is difficult to explore with high statistical relevance. In fact, the low forces region is located near the contact point, for distance $z < 15 \div 20$ nm, in which often the signal is masked by the presence of aspecific adhesion. Nevertheless, we recorded many curves in which the adhesion is low and the initial region can be explored, clearly showing a deviation of the curve from the WLC model (see Fig. 2) due to the presence of a residual force for $z \to 0$, which can be interpreted as the hallmark of the domain-domain interaction.

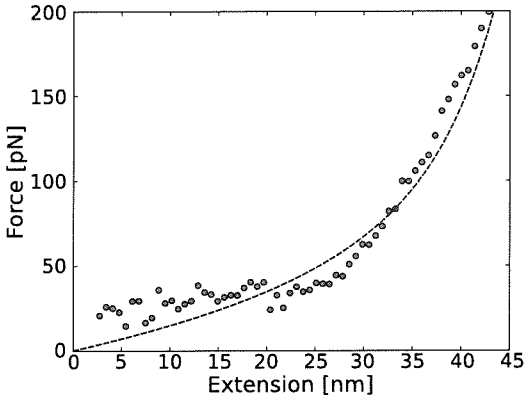

FIG. 2. (Color online) Zoom of the low forces region of a force versus distance curve on a single octamer molecule. The dashed line represents the WLC fit.

B. Small-angle x-ray scattering

In order to have a deeper insight into the structure of the octamer fragments, SAXS measurements were performed on two octamer samples with different concentrations: 50 and 230 mg/ml. Figure 3 shows the scattered intensity $I(Q)$ (in arbitrary units) as a function of scattering wave vector Q for the dilute and concentrated samples.

The increase of $I(Q)$ at low Q for the dilute solution is due to aggregates of octamers and will be discussed later. No preliminary filtration step was applied to this sample. The main characteristic of these curves is the presence of a very marked peak. The maximum and the width of the peak are closely related to the local order induced by electrostatic interactions. As the octamers are negatively charged (see caption of Table I), the octamer-octamer interactions are mainly due to excluded volume and screened Coulomb repulsions. In fact, there is a minimum in the potential energy at a definite interparticle distance, which depends on the specific volume fraction and charge of the molecules.

As shown in Fig. 3, with increasing the octamer's concentration or volume fraction η at a fixed pH, the peak shifts to higher Q values according to a general trend easily modeled for charged micellar solutions by Chen *et al.* [17,18]. Assuming a face-centered-cubic packing structure, where all the charged octamers are at the same distance from their first neighbors D, then

$$D = \frac{1}{\sqrt{2}}\left(\frac{4000}{N_A C_o}\right)^{1/3} 10^8 \text{ Å}, \tag{2}$$

where N_A is the Avogadro's number and C_o is the octamer's molar concentration.

In our case, we obtained $D = 348$ and 105 Å for dilute and concentrated samples, respectively. As expected, by increasing the volume fraction at a fixed pH, the mean interparticle distance D decreases. This approach has been already applied to very concentrated protein's solution of cytochrome C up to 0.5 in volume fraction and at different pH values [19,20].

It is worth noting that the SAXS curve of the dilute octamer shows an intensity increase at low Q, which is indicative of particles in solution larger than single octamers. This is not surprising since the sample has been analyzed after the sample preparation without any additional filtration step. To analyze the aggregation process in the dilute sample, a Guinier plot [21] was performed at low Q (see Fig. 4). At $QR < 1$ (where R is the radius of the aggregate), the Guinier equation $I(Q) = (\Delta\rho)^2 \exp[-(QR_g)^2/3]$ on the six first data points has a linear trend (see Fig. 4).

The Guinier radius $R_g = 124$ Å was calculated from the slope of the straight line in a $\ln[I(Q)]$ versus Q^2 plot. Assuming that the aggregates are spherical $R = R_g\sqrt{\frac{5}{3}}$, an average diameter of 320 Å can be extracted for the aggregates. This value found by SAXS at 20 °C on the dilute sample can be compared to those already reported in Ref. [10], where DLS results reveal 9% of aggregates of diameter 1580–2420 Å for the same case on the same sample at the same temperature. The intrinsic limit of a laboratory SAXS instrument is about 500–1000 Å, so that greater aggregates can not be seen even if present. On the other hand, it has been already shown [10] that the aggregation process is favored when the octamer fragment is denatured, leading to even greater aggregates. AFM results [10] confirm the presence of aggregates with a dimension of 2000–4000 Å near the octamer isoelectric point.

The Porod law [22] was used to find the background of the curve, assuming that the contrast between octamer and the solvent does not change with aggregation. By equation $Q^4 I(Q) = A + BQ^4$, the SAXS background was found and subtracted out along with the aggregates' contribution in the assumption of a polydisperse distribution of spheres (see the

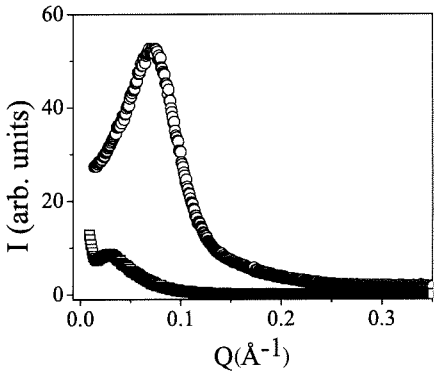

FIG. 3. Scattering intensity $I(Q)$ as function of scattering vector Q for dilute (experimental data: open square) and concentrated octamer's solutions (experimental data: open circle).

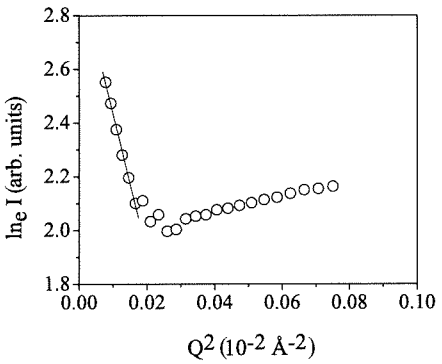

FIG. 4. (Color online) Guinier plot of dilute octamer sample.

details in the following). By DLS at 20 °C and 15 angular degrees (Ref. [10]), the scattered intensity is due to single octamers in solution (91%) and aggregates (9%). This implies that the aggregates are very few. Thus, it is reasonable to neglect the interactions between aggregates and also between aggregates and single octamers. For the dilute sample, we have simulated the SAXS curve of the aggregates using a model of spheres with Schulz polydispersity P_S on the radius [23], keeping fixed the average diameter of the aggregates and varying the amplitude factor and polydispersity. The Schulz distribution is a two-parameter function depending on the average diameter and Z_p related to polydispersity $P_S = 1/\sqrt{Zp+1}$, and is widely used for micelles and microemulsions [24,25].

This function is skewed toward larger sizes, tending to a Gaussian form at large values of Z_p. The polydispersity value of aggregates is 30%. After the aggregates' subtraction, the SAXS curve for the single octamer was obtained. When no aggregates are present, the scattered intensity of the samples can be calculated directly using the following equation [26]:

$$I(Q) = C_p(\Delta\rho)^2 v_p^2 M_p P(Q) S'(Q) + B, \qquad (3)$$

where C_p, v_p, and M_p are, respectively, the molar concentration, molecular volume, and molecular mass of the investigated octamer. $\Delta\rho = \rho_o - \rho_s$ is the excess scattering length density of octamer over the solvent. $P(Q)$ is the averaged intraparticle structure factor or form factor of a protein molecule over the ensemble of sizes and orientations, $S'(Q)$ is the effective interparticle structure factor, and B is the experimental background.

When considering particles that are polydisperse or nonspherical, such as protein molecules, the form factor varies from particle to particle. It is usually correct to assume that the particle orientations are completely uncorrelated with the particle positions; this hypothesis results in an average weighted by the distribution of particle sizes and orientations [27,28]:

$$S'(Q) = 1 + \beta(Q)[S(Q) - 1], \qquad \beta(Q) = \frac{|\langle F(Q)\rangle|^2}{\langle |F(Q)|^2\rangle}, \quad (4)$$

where

$$P(Q) = |\langle F(Q)\rangle|^2 = \left| \int_0^1 d\mu\, F(Q,\mu) \right|^2,$$

$$\langle |F(Q)|^2\rangle = \int_0^1 d\mu |F(Q,\mu)|^2. \qquad (5)$$

Two different form factors were taken into account considering, for the investigated octamer, both a globular and an extended conformation. This double approach is based on a series of experimental evidences already reported in the literature on similar systems.

The protein structure factor $S(Q)$ has been determined according to the generalized one-component macro-ion model (GOCM), an extension to the finite concentrations of the one-component macro-ion model (OCM) of Hayter and Penfold [29]. The so-called $\beta(Q)$ approximation has been applied as already reported [27].

For the globular conformation (see Appendix B for further details on the analytical framework), we took into consideration recent results reported by some of the authors [10], where DLS measurements suggested a very compact conformation for the I_{27}-I_{34} fragment with a hydrodynamic radius of $r_H = 25.9 \pm 0.4$ Å. Among simple globular shapes, best results were found by using a core-shell oblate ellipsoid (see Table I). The fitting curves of core-shell oblate ellipsoid are reported in Fig. 5 as a solid line. The agreement between the experimental curve and the model is poor only in the case of the more dilute sample in the very low Q region.

The parameters free to change independently are five: the overall octamer charge Z, the major and minor semiaxis of octamer a_p and b_p, the shell thickness t, and the quantity r, the ratio between the scattering length density of bound water molecule in the hydration shell and free water in the bulk. The background B was estimated by the Porod analysis at high Q values. The errors on these free parameters, reported in relative standard deviation, are, respectively, 7% for Z, 3% for t, 1% for a_p and b_p, and 2% for r.

The other calculated parameters shown in Table I are the axial ratio $\nu = a_p/b_p$, the effective hard sphere diameter σ_H, the volume fraction η, the screening parameter k, the Debye length l_D, and the contact potential γe^{-k}.

The screening parameter depends on the inverse screening length κ following the equations [30] $k = \kappa\sigma_H$, where

$$\kappa = \left(\frac{8\pi N_A e^2 I}{1000\epsilon_0\epsilon_r k_B T} \right)^{1/2}, \qquad (6)$$

e is the electronic charge, I is the ionic strength of the octamer solution, k_B is the Boltzmann constant, and ϵ is the dielectric constant of the medium at $T = 20$ °C. The Debye length of the interaction potential is related to the screening parameter k by the equation $l_D = \sigma_H/k$. Its value is $l_D = 15.2$ Å for the dilute solution and 5.5 Å for the more concentrated one. Only the shell thickness and Debye length differ for the dilute and concentrated octamer cases. Interestingly, the interfacial region and the Debye length of the octamer are more extended in the dilute case.

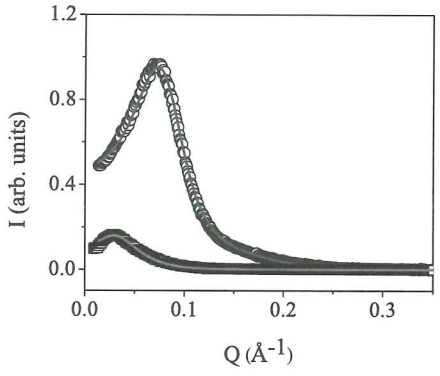

FIG. 5. (Color online) Scattering intensity $I(Q)$ as a function of scattering wave vector Q for dilute octamer solution (experimental data: open square) and concentrated octamer solution after subtraction of the aggregates' contribution (experimental data: open circle). The solid lines represent the fitted data according to a globular conformation interacting by a long-range repulsion potential.

The contact potential is

$$\gamma e^{-k} = \frac{(Ze)^2}{4\pi\epsilon k_B T \sigma_H (1 + k/2)^2}. \quad (7)$$

The structure and form factors $S(Q)$ and $P(Q)$ are extracted in both dilute and concentrated cases by using this first approach, and are shown in Figs. 6 and 7.

As reported in the literature [6,31,32], dilute solutions of short fragments from β-connectin I band can adopt extended arrangements with intrinsic flexibility where each Ig domain can be considered as a rigid repeating unit. In the attempt to better describe the more dilute case due to a modest agreement between the experimental curve and the core-shell oblate ellipsoid model, we decided to use a flexible cylinder model with a uniform scattering length density (for further details, see the Appendix of Ref. [33] and references therein).

The flexible cylinder is parametrized by a chain contour length L_{cyl}, a Kuhn length K_{cyl} used to describe the stiffness of a chain (i.e., the double of the length over which the flexible cylinder can be considered a rigid rod), and the radius of the cylinder cross section R_{cyl}. A polydispersity can be added to the cylinder length or to the cylinder radius according to the well-known Schulz distribution. This second approach was implemented with some approximations by modifying the small-angle neutron scattering (SANS) analysis package v7.0 [34], freely provided by NIST Center for Neutron Research (http://www.ncnr.nist.gov/programs/sans/data/red-anal.html) and simply combining the flexible cylinder's form factor with a screened Coulomb potential in the mean spherical approximation (MSA) [29] instead of using the rigorous approach of Ref. [33]. Figure 8 shows the fitting curves derived for flexible cylinders interacting via a long-range repulsion Coulombic potential as compared to the SAXS experiment.

The parameters charge L_{cyl}, R_{cyl}, and its polydispersity were left free to vary, while, from structural considerations [4], the Khun length was fixed *a priori* to the value of 86 Å, which is the double of the long axis of a β-connectin Ig domain. In Table II, the results of this second approach are reported for dilute and concentrated samples.

The error for L_{cyl} is ± 20 Å, for R_{cyl} is ± 0.2 Å, and for the charge ± 2. The cylinder radius agrees well with what has been already reported in the literature [31,32]. The cylinder length is closer to what is usually expected for tetramers. This

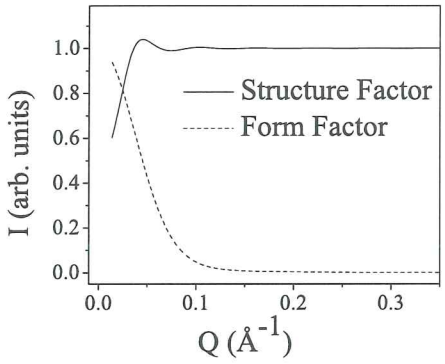

FIG. 6. $S(Q)$ (solid line) and $P(Q)$ (dashed line) curves for dilute octamer as determined by core-shell oblate ellipsoids interacting via a long-range repulsion Coulombic potential.

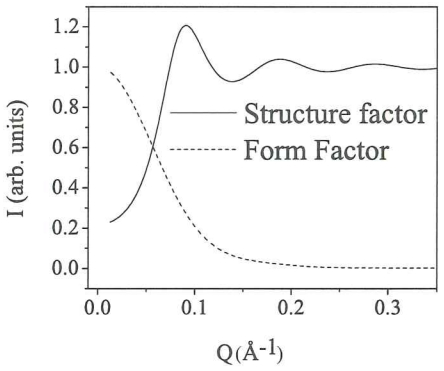

FIG. 7. $S(Q)$ (solid line) and $P(Q)$ (dashed line) curves for concentrated octamer as determined by core-shell oblate ellipsoids interacting via a long-range repulsion Coulombic potential.

disagreement can be due to the limited Q range achievable by the SAXS experiment and, moreover, to the fact that the structure factor in both samples dominates on the form factor contribution. In the dilute case, the aggregates' subtraction can be partially invoked to explain the reported differences. In order to reduce the structure factor contribution in favor of the form factor, a SAXS experiment in a more dilute sample is forecast. This can be measured in a synchrotron facility, while it is not achievable with the SAXS instrument used in the present case. It is worth noting that, anyway, very diluted samples can be far from the biological conditions.

The structure and form factors $S(Q)$ and $P(Q)$, as extracted by this second approach, for dilute and concentrated solutions are reported in Figs. 9 and 10.

V. DISCUSSION

The fitting results of Tables I and II for dilute and concentrated samples are very similar, suggesting that the structural parameters are quite independent from the sample concentration. In the core-shell oblate ellipsoid approach, the value of the effective hard sphere diameter, 49.0 Å (see Table I), is in agreement with the value of the hydrodynamic diameter

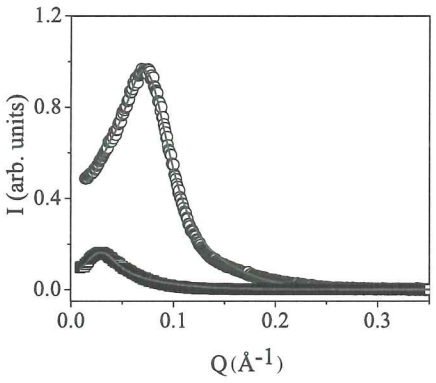

FIG. 8. (Color online) Scattering intensity $I(Q)$ as function of scattering wave vector Q for dilute octamer solution (experimental data: open square) and concentrated octamer solution after subtraction of the aggregates' contribution (experimental data: open circle). The solid lines represent intensity calculated for the flexible cylinders interacting via a long-range repulsion potential.

TABLE II. Fitting results using flexible cylinders interacting via a long-range repulsion term.

	Dilute	Concentrated
L_{cyl} (Å)	154	133
R_{cyl} (Å)	12.7	12.4
Polydispersity (P_S)	0.29	0.29
Charge (Z)	−11.0	−10.2
Monovalent salt (M)	0.002	0.010

$d_H = 51.8$ Å, found by DLS measurements [10], suggesting a very compact structure of the octamer.

However, in Ref. [32], a fairly extended arrangement of all Ig domains in an I-band poly-Ig fragment is proposed where the average length of one Ig domain is 44 Å. According to this hypothesis, we decided to use also the flexible cylinder's model. The values reported in Table II partially confirm the results of Refs. [6,31,32]. In fact, the value of R_{cyl} corresponds to the axial dimension of a single Ig domain as reported in [31]. The L_{cyl} value agrees with the $d_{max} = 150$ Å reported in [31] and 230 Å [32] for fragments composed by four and six Ig domains, respectively. In our case, we expected a greater value for L_{cyl} but, according to a torsion of the octamer path from linearity, as proposed in Ref. [6], it is reasonably a conformational freedom in the fragment, allowing a certain degree of bending between Ig domains, thus, a more compact structure.

This argumentation suggests a shortening of Ig-domain fragments compared to the length of a single Ig domain due to a progressive shrinking, as more domains are included in the fragments. Also, according to the model of elasticity proposed in Ref. [6], it is possible to localize flexible points along the overall fragments, leading to a reorganization of the three-dimensional structure of fragment in solution. The theoretical octamer charge value can be calculated using the pK_a values for the individual amino acid residues at the solution pH. For a folded protein, the latter statement is not valid. However, this rough value can be useful as a starting point in any fitting procedure. Protein Calculator v3.3 [12] gives an estimated charge of about −18.8 at pH 7.4, higher than what was obtained from the two fitting procedures used in this paper (see Tables I and II).

This result is in agreement with the fact that the octamer charge Z is not the total charge on the octamer surface, but the charge experienced by the octamer. This value is usually lower than the theoretical one according to the well-known charge renormalization phenomenon [35], which microscopically can be visualized as resulting from a piling up of the counterions near the octamer surface. As far as the interaction of an octamer molecule with another octamer molecule sitting at some distance is concerned, part of the piled-up counterions near the surface adsorbs at the interface and, in this way, reduces the effective surface charge.

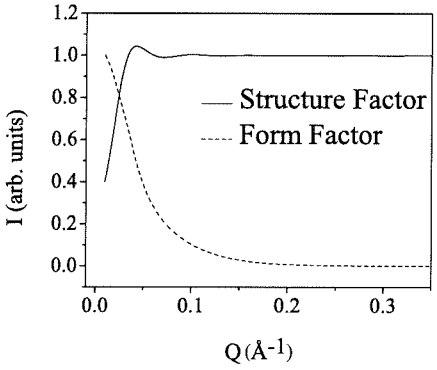

FIG. 9. Fitted $S(Q)$ (solid line) and $P(Q)$ (dashed line) curves for dilute octamer by the flexible cylinder's model.

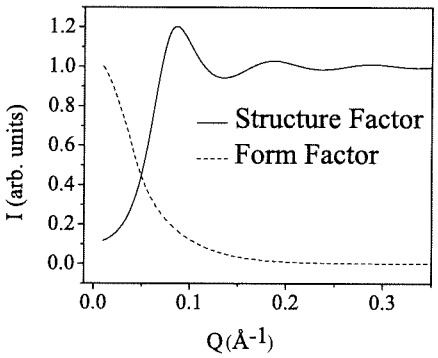

FIG. 10. Fitted $S(Q)$ (solid line) and $P(Q)$ (dashed line) curves for concentrated octamer by the flexible cylinder's model.

In addition, we have to stress that, by using the two fitting approaches, the octamer's charge values are in good agreement within the error limits. Also, the flexible cylinder's model fits well the experimental SAXS curves by introducing a very small salt concentration, likely due to a salt residual remaining in solution after the affinity chromatography procedure.

By performing single-molecule force spectroscopy experiments on the octamer sample, the mechanical unfolding properties were analyzed. In the single-molecule stretching events, the force-extension curve showed the characteristic regular sawtooth pattern shape, providing a clear indication that the recorded force-extension profiles were derived from a modular protein, as was the octamer.

Furthermore, WLC fitting analysis was performed, highlighting a purely entropic spring behavior for the investigated protein fragments in the high forces regimes (the peaks). In this regard, both the maximum rupture force of each peak and the persistence lengths were estimated and found to be in good accord with the values found for the polypeptide composed by eight repetitions of Ig_{27} domain of β-connectin protein [8,9].

The region for low displacements of the force versus distance curves was observed in more detail, showing the presence of many deviations from the purely entropic WLC model and giving an indication of the presence of much weaker interaction than that associated to unfolding events.

VI. CONCLUSION

Fragments of the muscle cardiac protein β-connectin, belonging to the I band of the sarcomer, composed of eight Ig domains from I_{27} to I_{34}, named octamer fragments, were investigated by SAXS and SMFS by AFM with the purpose to characterize the microstructure of the octamers and their mechanical and elastic properties. The presence of a third type of elasticity in the molecule β-connectin, associated to the domain-domain interaction, has been proposed on the basis of numeri-

cal simulations [7]. AFM stretching experiments performed on a Ig_{27}-Ig_{34} octamer show that the lower forces region is not approximated with the standard WLC model as well as the higher forces regimes, thus indicating that a residual, nonentropic elasticity can be, in fact, individuated. This behavior suggests that the modules are mutually interacting, probably leading to a organized three-dimensional structure in solution, and this hypothesis has been investigated using SAXS spectroscopy.

By SAXS, it was possible to know the octamer's charge, shape, size, Debye length, and contact potential in the case of ellipsoids interacting via a long-range repulsion potential formalized by GOCM's approach, and the charge, cylinder length, cross-section radius, and its polydispersity in the case of the flexible cylinder's interacting with the same potential on two octamer samples at different concentrations, 50 and 230 mg/ml.

To analyze the SAXS curve of the dilute octamer, it was mandatory to subtract the contribution of the octamer's aggregates, measuring their average gyration radius in the Guinier approximation. Then, we performed the aggregate subtraction in the intensity distribution, assuming the octamer aggregates' fraction to be composed by polydisperse spheres. Once found, the dilute sample SAXS curve without the octamer's aggregates' contribution was analyzed by the core-shell oblate ellipsoid and flexible cylinder's approaches. The concentrated octamer sample does not present aggregates, thus, the SAXS intensity was analyzed directly by both models.

The results of the SAXS experiments combined with them from the AFM stretching experiments on a Ig_{27}-Ig_{34} octamer can offer the possibility to determine the way in which the Ig domains are assembled in a modular protein such as β-connectin and to understand whether the consecutive Ig domains are free to move with respect to one another, leading to the reorganization of the shape and the structure of the whole protein. The results, suggesting mutual domain orientations and their interactions, might help us in understanding more about the nature of domain-domain interactions in the β-connectin, eventually suggesting a localization of flexible points along the total fragment under consideration.

These arguments can offer great promise in the modeling of the stretch-response mechanism of the poly-Ig domains in the muscle and allow us to consider their overall elasticity, a critical parameter for specific functions of these systems in biotechnological and pharmaceutical applications.

ACKNOWLEDGEMENT

The authors kindly acknowledge the Ente Cassa di Risparmio di Firenze, the Consorzio Interuniversitario per lo Sviluppo dei Sistemi a Grande Interfase (CSGI), and the Ministero dell'Istruzione, dell'Università e della Ricerca (MIUR) for financial support.

APPENDIX A

β-connectin fragments were amplified by reverse transcription and polymerase chain reaction (RTPCR) from 1 μg of human cardiac total RNA using the SuperScript one-step RT-PCR kit (Invitrogen, Milan, Italy), according to the manufacturer's instructions. The PCR primers flanking the I_{27}-I_{34} fragment were designed according to the published human cardiac β-connectin cDNA sequence (Gen-Bank accession number X90568) in order to obtain a COOH-terminal Cys^2 tag for immobilization on solid surfaces. The PCR products of the expected size 2144 base pairs for the I_{27}-I_{34} fragments were identified by agarose gel electrophoresis and then cloned into the Champion pET 100 Directional TOPO vector (Invitrogen, Milan, Italy), fused with an NH_2-terminal His^6 tag for fragment purification. The identity of the cloned fragments was verified by DNA sequencing with the use of a standard automated sequencer. Expression of the fragments was induced in BL21(DE)3 cells by 0.1 mM isopropyl-β-D-thio-glactopyranoside (IPTG) at 37 °C for 4 h. The proteins were expressed in soluble form and were purified by Ni affinity chromatography (Novagen, Milan, Italy), according to the protocol provided by the manufacturer. Fusion proteins were eluted in buffer solution of 50 mM Tris-HCl, 0.5 M NaCl, and 80 mM ethylene diamine tetra-acetic acid with pH = 8.0 and Debye screening length 0.41 nm. It is notable that the pH of these protein solutions is 7.34 measured by Metrohm glass electrode PH-207. This value is higher than pH = 5.8, the isoelectric point of the protein, i.e., the pH at which a protein carries no net charge, calculated using Protein Calculator v3.3 [12].

APPENDIX B

Considering the surface of protein very complex, as suggested by Svergun *et al.* [36], to improve the agreement between the experimental and calculated x-ray scattering curves, we have taken into account the existence of a hydration shell coming from the adsorption of water molecules at the protein surface. This border layer has a scattering density typically ≈1.05–1.25 times that of the bulk. Hence, a two-shell model is used as form factor. Assuming that protein adopts a globular oblate (axis a,a,b) or prolate (axis a,b,b) ellipsoidal shape, we have

$$F(Q,\mu) = (\rho_o - \rho_{\rm sh})V_p[3j_1(u_p)/u_p] + (\rho_{\rm sh} - \rho_s)V_t[3j_1(u_t)/u_t], \tag{B1}$$

where

$$u_p^{\rm obl} = Q[b_p 2\mu 2 + a_p 2(1-\mu 2)]^{1/2}, \quad u_p^{\rm prol} = Q[a_p 2\mu 2 + b_p 2(1-\mu 2)]^{1/2}, \tag{B2}$$

$$u_t^{\rm obl} = Q[b_t 2\mu 2 + a_t 2(1-\mu 2)]^{1/2}, \quad u_t^{\rm prol} = Q[a_t 2\mu 2 + b_t 2(1-\mu 2)]^{1/2}. \tag{B3}$$

Here, ρ_o, $\rho_{\rm sh}$, and ρ_s are the scattering length densities of octamer, hydration shell, and solvent, respectively. μ is the cosine of the angle between the scattering vector Q and the major axis of the ellipsoid and $j_1(x)$ is the first-order spherical Bessel function.

The major semiaxis a_t is given by $a_t = a_p + t$, where a_p is the major semiaxis of dry octamer and t is the thickness of the hydration shell. Similarly, the minor semiaxis b_t is given by $b_t = b_p + t$ and b_p is the minor semiaxis of dry octamer. The volume of dry octamer V_p and the overall volume of the octamer considering the hydration shell V_t are, respectively,

given by

$$V_p^{\text{obl}} = (4/3)\pi {a_p}^2 b_p, \qquad V_t^{\text{obl}} = (4/3)\pi {a_t}^2 b_t, \quad \text{(B4)}$$

$$V_p^{\text{prol}} = (4/3)\pi a_p {b_p}^2, \qquad V_t^{\text{prol}} = (4/3)\pi a_t {b_t}^2. \quad \text{(B5)}$$

The values of effective hard sphere diameters of octamer in the two cases are

$$\sigma_H^{\text{obl}} = 2({a_p}^2 b_p)^{1/3}, \qquad \sigma_H^{\text{prol}} = 2(a_p {b_p}^2)^{1/3}. \quad \text{(B6)}$$

[1] K. Maruyama, Int. Rev. Cytol. **104**, 81 (1986).
[2] H. Higuchi, Y. Nakauchi, K. Maruyama, and S. Fujme, Biophys. J. **65**, 1906 (1993).
[3] L. Tskhovrebova and J. Trinick, Nat. Rev. Mol. Cell Biol. **4**, 679 (2003).
[4] S. Improta, A. S. Politou, and A. Pastore, Structure **4**, 323 (1996).
[5] S. Labeit and B. Kolmerer, Science **270**, 293 (1995).
[6] E. von Castelmur, M. Marino, D. I. Svergun, L. Kreplak, Z. Ucurum-Fotiadis, P. V. Konarev, A. Urzhumtsev, D. Labeit, S. Labeit, and O. Mayans, Proc. Natl. Acad. Sci. USA. **105**, 1186 (2008).
[7] E. H. Lee, J. Hsin, E. von Castelmur, O. Mayans, and K. Schulten, Biophys. J. **98**, 1085 (2010); J. Hsin and K. Schulten, *ibid.* **100**, L22 (2011).
[8] M. Rief, M. Gautel, F. Oesterhelt, J. M. Fernandez, and H. E. Gaub, Science **276**, 1109 (1997).
[9] A. Imparato, F. Sbrana, and M. Vassalli, Europhys. Lett. **82**, 58006 (2008).
[10] S. Marchetti, F. Sbrana, R. Raccis, L. Lanzi, C. M. C. Gambi, M. Vassalli, B. Tiribilli, A. Pacini, and A. Toscano, Phys. Rev. E **77**, 021910 (2008).
[11] S. C. Gill and P. H. von Hippel, Anal. Biochem. **182**, 319 (1989).
[12] [http://www.scripps.edu/ cdputnam/protcalc.html].
[13] E. Mylonas and D. I. Svergun, J. Appl. Crystallogr. **40**, s245 (2007).
[14] T. N. Blanton, T. C. Huang, H. Toraya, C. R. Hubbard, S. B. Robie, D. Louer, H. E. Gobel, G. Will, R. Gilles, and T. Raftery, Powder Diffraction **10**, 91 (1995).
[15] J. A. Lake, Acta Crystallogr. **23**, 191 (1967).
[16] C. Bustamante, S. B. Smith, J. Liphardt, and D. Smith, Curr. Opin. Struct. Biol. **10**, 279 (2000).
[17] S. H. Chen and E. Y. Sheu, in *Micellar Solutions and Microemulsions: Structure, Dynamics, and Statistical Thermodynamics*, edited by S. H. Chen *et al.* (Springer, New York, 1990).
[18] S. H. Chen, E. Y. Sheu, J. Kalus, and H. Hoffmann, J. Appl. Crystallogr. **21**, 751 (1988).
[19] P. Baglioni, E. Fratini, B. Lonetti, and S. H. Chen, J. Phys. Condens. Matter **16**, S5003 (2004).
[20] B. Lonetti, E. Fratini, S. H. Chen, and P. Baglioni, Phys. Chem. Chem. Phys. **6**, 1338 (2004).
[21] A. Guinier and G. Fournet, *Small-Angle Scattering of X-Rays* (Wiley, New York, 1955).
[22] O. Glatter and O. Kratky, *Small Angle X-Ray Scattering* (Academic, New York, 1982).
[23] M. Kotlarchyk and S. H. Chen, J. Chem. Phys. **79**, 241 (1983).
[24] L. Scaffei, L. Lanzi, C. M. C. Gambi, R. Giordano, P. Baglioni, and J. Teixeira, J. Phys. Chem. B **106**, 10771 (2002).
[25] C. M. C. Gambi, R. Giordano, M. Laurati, L. Lanzi, F. Pini, and P. Baglioni, Appl. Phys. A: Mater. Sci. Process. **74**, S377 (2002).
[26] R. Nossal, C. J. Glinka, and S. H. Chen, Biopolymers **25**, 1157 (1986).
[27] S. H. Chen, Annu. Rev. Phys. Chem. **37**, 351 (1986).
[28] S. Khan, T. L. Morton, and D. Ronis, Phys. Rev. A **35**, 4295 (1987).
[29] J. P. Hansen and J. B. Hayter, Mol. Phys. **46**, 651 (1982).
[30] R. J. Hunter, *Foundations of Colloid Science* (Clarendon Press, Oxford, 1987), Vol. I.
[31] S. Improta, J. K. Krueger, M. Gautel, R. A. Atkinson, J. F. Lefevre, S. Moulton, J. Trewhella, and A. Pastore, J. Mol. Biol. **284**, 761 (1998).
[32] M. Marino, D. I. Svergun, L. Kreplak, P. V. Konarev, B. Maco, D. Labeit, and O. Mayans, J. Muscle Res. Cell Motil. **26**, 355 (2005).
[33] W. R. Chen, P. D. Butler, and L. J. Magid, Langmuir **22**, 6539 (2006).
[34] S. R. Kline, J. Appl. Crystallogr. **39**, 895 (2006).
[35] C. F. Wu and S. H. Chen, Biopolymers **27**, 1065 (1988).
[36] D. I. Svergun, S. Richard, M. H. J. Koch, Z. Sayers, S. Kuprin, and G. Zaccai, Proc. Natl. Acad. Sci. USA. **95**, 2267 (1998).